Easy Processable Photomechanical Thin Film Involving a Photochromic Diarylethene and a Thermoplastic Elastomer in Supramolecular Interaction

Ismael Arroyo Diaz, Rebeca Cedeno Madera, Nour Nour Eddine, Gilles Alcaraz, Sandrine Pensec, Laurent Bouteiller, Moussa Nait Abdelaziz, Sophie Barrau, Jean-Francois Tahon, David Fournier, et al.

Easy processable photomechanical thin film involving a photochromic diarylethene and a thermoplastic elastomer in supramolecular interaction

Ismael Arroyo[a], *Rebeca Cedeño*[b], *Nour Nour Eddine*[c,d], *Gilles Alcaraz*[c], *Sandrine Pensec*[d], *Laurent Bouteiller*[d], *Moussa Naït-Abdelaziz*[b] , *Sophie Barrau*[e], *Jean-François Tahon*[e], *David Fournier*[e], *Alexandre Fadel*[f], *Michinori Takeshita*[g], *Guy Buntinx*[a] *and Stéphane Aloïse**[a]

[a]Université de Lille, CNRS, UMR 8516 – LASIRE – Laboratoire de Spectroscopie pour les Interactions, la Réactivité et l'Environnement, 59000 Lille, France.
[b]Université de Lille, Unité de Mécanique de Lille-Joseph Boussinesq ULR 7512, 59000 Lille, France
[c]Univ Rennes, CNRS, ISCR (Institut des Sciences Chimiques de Rennes) – UMR 6226, F-35000 Rennes, France.
[d]Sorbonne Université, CNRS, Institut Parisien de Chimie Moléculaire, Equipe Chimie des Polymères, 4 Place Jussieu, 75005 Paris, France.
[e]Université de Lille, CNRS, INRAE, Centrale Lille, UMR 8207 – UMET – Unité Matériaux et Transformations, F-59000 Lille, France.
[f]Université de Lille, CNRS, INRAE, Centrale Lille, Univ. Artois, FR 2638 - IMEC – Institut Michel-Eugène Chevreul, F-59000 Lille, France
[g]Department of Advanced Technology and Fusion, Graduate School of Science and Engineering, University of Saga, Japan.

*corresponding authors: stephane.aloise@univ-lille.fr;

Keywords: *photoactuators, photomechanical effect, Photochromism, thermoplastic elastomer, DTE, UPy, supramolecular interaction*

Abstract

As an alternative to liquid crystal elastomers (LCE) involving azobenzene (AZO) units or photochromic microcrystals, a novel supramolecular photoactuator is presented in the shape of a thin film with centimetric size. The thin film is easily obtained by spin coating and does not require any alignment or crosslinking processes. Chemically, this photoactuator combines a photochromic dithienylethene (A) functionalized with ureidopyrimidinone (UPy) units with a telechelic thermoplastic elastomer (B) functionalized with UPy units as well, allowing the connections of the two compounds via quadruple hydrogen bonds. Upon alternating UV/visible light irradiation, a reversible bending/flattening movement was observed together with a reversible change of color. Both processes were studied using a displacement and absorption tracking setup. The photomechanical effect (PME) has been rationalized through kinetic analysis and combining distinct material science techniques

implementing in-situ illumination. The PME is explained in terms of photoinduced strain generated inside 160 nm UPy-bonded dithienylethene domains that reversibly expand and contract (by about 50%) under UV and visible light, respectively. The semi-crystallinity of the elastomer and a strong supramolecular network connecting both A and B have been identified as important parameters to efficiently turn the microscopic photo-strain into macroscopic actuation. If the performances of the supramolecular actuator are not comparable to those of state-of-the-art LCE-AZO systems (low power light were favored), potential improvements are discussed for the future.

1. Introduction

Over the past two decades, there have been extensive global efforts to develop smart materials that respond to external stimuli such as heat,[1] electricity,[2] magnetic fields,[3] humidity,[4] or light.[5] These technological advances have impacted various industrial sectors, including environmental issues,[6] biotechnology, health monitoring,[7] engineering,[8] soft robotics,[9] and the textile industry.[10] Photoresponsive materials,[11–13] such as photomechanical materials, offer advantages over other stimuli due to their wireless controllability and spatial selectivity. In addition, the stimuli can be tuned by changing the intensity, the wavelength, or even the polarization of the light.[14] Given their ability to convert light energy into mechanical forces, these materials have gained increasing interest from both academic and practical perspectives.[13] Materials that exhibit a photomechanical effect (PME) under irradiation[14–17] can be classified according to their actuation mechanisms: i) photoelectric processes, which are mostly found in inorganic solids;[18,19] ii) photothermal processes for dye-containing systems;[20,21] iii) photochemical systems that involve only an organic photoswitch -the so-called dynamic crystals-[22–24] or photochromic units embedded in a polymeric matrix.[25–27] In this article, we will focus on the latter class of systems. Several families of photochromic compounds, including spiropyrans and fulgides, have been tested for the development of photoactive materials.[28,29] However, two molecules have particularly caught the interest of researchers: diarylethene (DAE) and dithienylethene (DTE) derivatives due to their bistability and high fatigue resistance[30] and azobenzene (AZO) derivatives, which undergo significant molecular geometry changes during trans/cis photoisomerization, resulting in substantial deformation of materials.[31,32]

For AZO derivatives, fibers,[33] functionalized polyimides,[34] or functionalized polymer networks[33,35] have shown promising PME but limited to less than 1%

photoinduced shrinking. To increase efficiency, a straightforward approach was to align and orient the photoresponsive units. With the development of liquid crystal elastomers (LCE),[36] improvements in photomechanical effects have been achieved by aligning the mesogens using methods such as electric fields, magnetic fields, external stretching, and appropriate glass cell coatings.[37–40] Since 2001, Finkelmann et al. have been pioneering in introducing new functionality to the well-known thermomechanical LCE by demonstrating reversible macroscopic shape changes through photoisomerization of nematic monodomains.[41] Ikeda's group achieved further improvement by synthesizing multi-domain LCEs using thermally polymerized liquid crystal monomers and crosslinkers based on azobenzene derivatives.[42] The high concentration of AZO units limits light penetration to the surface and induces a bending or flattening behavior of the thin film under UV or visible irradiation, respectively.[42–45] To increase the durability of the final photoactuator, composite systems with an additional flexible plastic film (polyethylene) have been investigated to produce the first light-operated motors reported in the literature.[44,46] To date, the PME reported for LCE-AZO systems is the most efficient, but it has two major drawbacks: i) the presence of thermal back-reaction for AZO units (as they are not bistable photoswitches) and ii) the need for an additional processing step for mesogen alignment and film cross-linking. The first question was recently addressed by Lahikainen et al. They replaced the AZO with DTE units[47] to tune the photothermal effect of the LCE. More recently, Hebner et al.[48] prepared DAE-LCE containing thiol-anhydride linkages to elaborate a photoactuator with good performances under UV or visible irradiation. The photoactuator showed almost 6% photostrain over 5 photochromic cycles. This approach utilizes thiol-anhydride dynamic bonds within the network structure to align the LCE and maintain its shape after initial deformation. However, it is important to note that some temperature elevation up to 80°C is still necessary to activate the dynamic chemistry. In terms of processing complexity (see Zhao et al.[49] for a review), Ube et al. recently studied a thermoplastic polyurethane containing AZO units in the backbone to achieve reversible photoactuation and versatile processability without the need for a covalent crosslinking step. The macroscopic shape was controlled by the formation of physical cross-links through hydrogen bonding interactions. However, alignment under mechanical stretch at 90°C was still necessary.[50]

The substitution of covalent cross-linking with supramolecular interactions or dynamic networks presents a promising strategy for achieving simpler processability and promoting recyclability.[51,52] The study of supramolecular bonds in photoactive polymeric materials

has included hydrogen-type bonds,[53–55] halogen bonds,[56] coordination bonds,[57] ionic interactions,[58] charge transfer interactions[59], and host-guest interactions.[60] In particular, the synthesis of 2-ureido-4[1H]-pyrimidinone (UPy units) by Meijer and coworkers[61–63] has opened the door to the formation of supramolecular polymers based on quadruple hydrogen bonds and their ability to be attached to side groups of the polymer backbone or as telechelic units.[54,55] To generate good flexible materials, the functionalization of copolymers such as poly(ethylene-co-butylene) (PEB) with UPy units, noted in the following **Elastomer B** (see Figure 1) was first performed by Meijer et al.[64] with an amorphous microstructure and the semi-crystalline analog was recently reported[65] depending on the extent of ethylene content (hard fragment) concerning butylene units (soft fragment). In this case, Differential Scanning Calorimetry (DSC) and Small/Wide Angle X-ray Scattering (SAXS/WAXS) techniques demonstrated a double physical cross-linking through polyethylene crystallites and UPy-UPy stacking units.[64,65] Takeshita et al. have recently reported the synthesis of a photochromic molecule called DTE derivative, which has been functionalized on both sides with UPy groups. This **Photoswitch A** (refer to Figure 1) has self-assembly kinetic driven by irradiation.[66,67] According to ultrafast spectroscopy, the supramolecular self-assembly process does not significantly affect the primary photoswitching processes in the solution.[68]

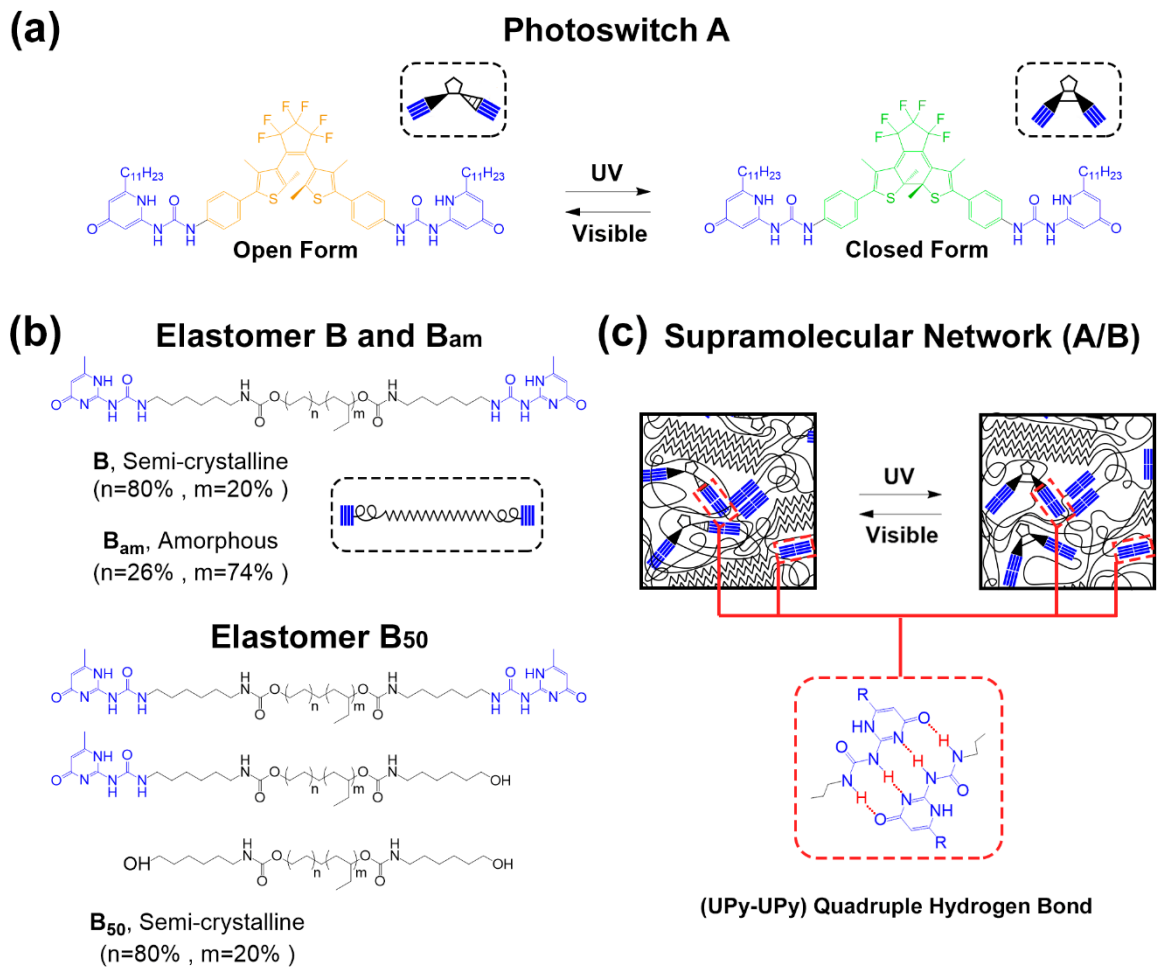

Figure 1. Molecular structure of a) isomers of dithienylethenes functionalized with UPy (A) in open (OF) and closed (CF) forms, b) poly(ethylene-co-butylene) fully functionalized semi-crystalline (B) with UPy, 50% functionalized semi-crystalline (B_{50}) and fully functionalized amorphous (Bam). c) Illustration of supramolecular self-assembly between A and B through quadruple hydrogen bonding linking two UPy moieties.

The objective of the present work was to create a new type of photo-actuator using a simple and fast processing method that doesn't require any alignment steps. We combined a photoswitch (A) with a thermoplastic elastomer (B) to create a supramolecular polymer network (A/B) that uses quadruple hydrogen bonding of UPy units. Our goal was to use the versatility of supramolecular chemistry and the performance of DTE units to create a reversible photoactuator that is solely controlled by light, without any participation of photothermal effects. Furthermore, we present the PME for our new class photoactuator with special attention given to structural and morphological rationalization. The importance of the elastomer microstructure and efficient UPy network is demonstrated.

2. Results and discussion

2.1. Processing and tracking setup

Processing is remarkably simple: photoswitch A and elastomer B are mixed in chloroform solution and then spin-coated on silicone paper. Free-standing strips (10 mm x 2 mm x 20 µm) are cut from the spin-coated thin film (A/B) and maintained in a vertical position by a tweezer (Figure 1a). The thin film obtained is photochromic, the open form (OF) being colorless and the closed form (CF) being blue (as expected from the solution study)[68] with an absorption maximum near 600 nm as shown in Figure 1b. Before starting measurements, a period of 24 hours of rest is imposed (thin film in a vertical position held by tweezers) to release any residual mechanical stress (from substrate peeling, tweezers constrain). Then, each system is characterized according to the displacement tracking profile (video) and absorbance tracking profile (laser and photodiode) described in the experimental section.

2.2. Photoactuation vs Photochromism

The performance of the photoactuator is shown in Figure 2c for both the displacement tracking profile (black curve) and the absorbance tracking profile at 635 nm (red curve) during 6 cycles of 1 hour of visible or UV illumination. The supporting information section S2 includes Video S1 of the tracking profile. Two snapshots of the video are shown in Figure 2a, while the maximum displacement for each cycle is shown in Figure 2d.

Focused on Figure 2c, the displacement and absorption tracking profiles show similar trends, indicating a strong correlation (see below). Initially, the thin film (A/B) with the OF photochromic units is non-reactive during the first visible irradiation because the film is colorless (verification stage). When the light is switched to UV, the film displaces 375 µm to the right (toward the light direction) and turns blue during the OF→CF photoconversion. Upon exposure to visible light, the film returns to its initial absorbance value (OF) and moves backward along a 475 µm distance. The forward and backward movement is reported on five occasions, providing evidence for the reversibility associated with the photoconversion processes of A. It should be noted that the decreasing intensity for the absorbance tracking curve (Figure 2c) is not related with photodegradation. Indeed, we took advantages of the supramolecular property of the (A/B) system by redissolving the thin film in chloroform to make sure that the absorbance after 6 cycles was unaltered compare to the starting material. Instead, this decrease of intensity is due to a screening effect related to small percentage of unconverted CF (around 10%) after one full UV/Visible cycle (OF→CF→OF). The residual CF absorbs UV light too and conscequently decrease the number of UV photons available for

the photoconversion process of the OF decreasing logically the CF quantity. Unlike solution, full conversion of photochromic thin film takes very long time but we restrict the irradiation period (1h) to avoid relaxation of the elastomeric matrix. In the following, we expect that the screening effect may influence the photomechanical behavior.

As shown in Figure 2d, the extent of the displacement remains constant for visible illumination, with a mean displacement of ~480 µm. With UV excitation, the displacement first increases for the initial two cycles, peaking at 600 µm, and subsequently decreases to 390 µm continuously. Anyhow, the proximity of the two displacement values permits achieving the desired reversibility at the macroscale in comparison to DTE monocrystals.[69]

Before proceeding with the analysis, it is important to clarify that no thermal process could have caused the reported displacements. Indeed, during a long illumination sequence with a consistent LED power of 1 $mW.cm^{-2}$, the temperature of the photoactuator was measured using a thermal camera. The temperature ranged between 23° and 27°, as shown in Video S2 and S3 available in Supporting Information S5. Therefore, this system is exclusively controlled by the photochemistry of the photoswitch.

In terms of the bending velocity performances, the present system runs at around 0.1 $µm.s^{-1}$ for both UV and visible irradiations. At first glance, these performances seem to be far from recent state-of-the-art LCE-AZO systems with similar thicknesses, (70 $µm.s^{-1}$ for UV @ 10 $mW.cm^{-2}$ and 10 $µm.s^{-1}$ for visible at 40 $mW.cm^{-2}$).[50] However, we must take into account that our illumination conditions are much lower (1 $mW.cm^{-2}$) than those used in other studies, which explains the difference in results. However, even with a moderated range, we obtain strong evidences that photomechanical effect is linearly proportional to the power of the LED for both that UV and Visible excitation (see Supporting Information S6) which confirm that the photochromic units play a central role within PME. The much higher slope for the UV light compare to visible excitation is in adequation with the higher quantum yield expected for photocyclisation compare to photoreversion. [REF HAMDI 2019] Furthermore, unlike other systems, we do not proceed with additional heating during the photoactuation cycle. Anyhow, as already mentioned, more than improving performances, we are interested in proposing a novel alternative and easy processable system.

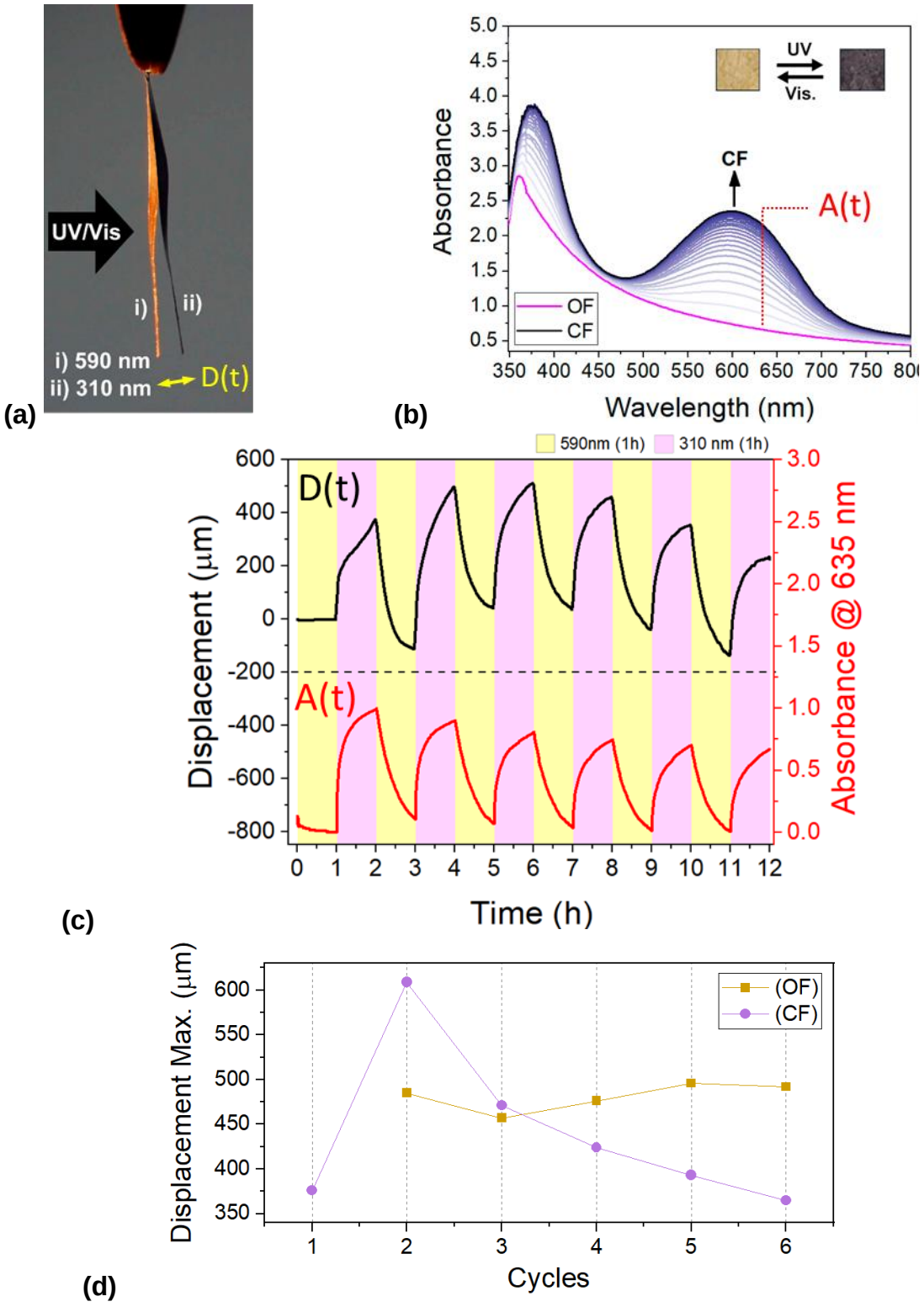

Figure 2. (a) Snapshots from Video S1 showing the position of the thin film (A/B) at the end of the first visible and UV illumination cycle (1 hour each). (b) Absorbance spectra of thin film (A/B) under gradual illumination with UV. (c) Displacement tracking profile (black curve) and absorbance tracking profile (red curve) for an initial colorless thin film (A/B) during 6 cycles of irradiation (1 hour) with UV (310 nm) and visible light (590 nm) with moderated LED power (1 mW.cm^{-2}). The dimensions of the thin film are (10 x 2 x 0.017) mm^3.(d) Maximum magnitude of the displacement for each UV (purple) and visible (orange) cycle.

Kinetic Analysis. The mechanical response of our system is controlled by the photochemistry of the A units across the film, similar to DTE monocrystals,[70] since we have excluded any photothermal contributions. Therefore, to quantitatively correlate the PME with the photochromic gradient CF/OF across the film, subsequent kinetic analyses of both the displacement and absorbance tracking profiles were performed. After testing the multi-exponential function, it was found that both the displacement *D=f(t)* (black curve in Figure 2c) and absorbance *A=f(t)* (red curve in Figure 2c) tracking profiles are best fitted with a double exponential function for UV excitation and a mono-exponential function for visible illumination, as shown on the equations below:

$$UV \rightarrow \quad D(t) \propto a_1^D e^{-\frac{t}{\tau_1^D}} + a_2^D e^{-\frac{t}{\tau_2^D}} \qquad vs \qquad A(t) \propto a_1^A e^{-\frac{t}{\tau_1^A}} + a_2^A e^{-\frac{t}{\tau_2^A}} \qquad (1)$$

$$Visible \rightarrow \quad D(t) \propto a_3^D e^{-\frac{t}{\tau_3^D}} \qquad vs \qquad A(t) \propto a_3^A e^{-\frac{t}{\tau_3^A}} \qquad (2)$$

where τ_i^X and a_i^X (index=1,2 for UV and i=3 for Visible; suffix X = A for absorbance or D for displacement) are characteristic times and pre-exponentials factors respectively. Such particularity (mono vs double exponential) has been reported in the past for spiropyran microcrystals[71] or amorphous DTE.[72] The justification for the bi-exponential behavior in UV versus the mono-exponential behavior in visible light can be explained through the mathematical model developed by Bertarelli *et al.* [REF Bertarelli] In essence, the first exponential depend solely on the photoconversion rate while the second exponential term includes the contribution of the elastomer absorbing a portion of the UV light, a process absents for visible light. Note that other factors can contribute to this second exponential term like the antiparallel/parallel ratio [REF IRIE] or the photoenolization of the UPy units. [REF photoenolization] However, beyond the physical explanation of this result, our purpose is to assess the possible quantitative correlation between both photomechanical and photochromic processes.

Table 1. Characteristic times (τ_1^A, τ_2^A) and (τ_1^D, τ_2^D) were deduced from fitting the absorbance and displacement tracking profiles for each UV cycle respectively with a biexponential function. Characteristic times (τ_3^A) and (τ_3^D) were deduced from fitting the absorbance and displacement tracking profiles for each Visible cycle respectively with a mono-exponential function.

	Absorbance tracking profile A(t)			Displacement tracking profile D(t)		
	UV		Vis	UV		Vis
Cycle	τ_1^A [min]	τ_2^A [min]	τ_3^A [min]	τ_1^D [min]	τ_2^D [min]	τ_3^D [min]
1	1.2	18	-	-	-	-
2	1.3	19	28.8	4.4	50	16.1
3	2.1	26	28.3	4.9	47	17.4
4	2.2	28	26.9	5.3	36	19.5
5	2.4	32	26.1	6.2	39	21.0
6	2.8	35	25.9	5.6	23	21.9

Let us first analyze the photoreversion case (visible illumination). From cycle #1 to cycle #6, as seen in Table 1, the characteristic time τ_3^A (< 22 min) decreases for the discoloration kinetic when τ_3^D (< 26 min) is increasing for the displacement, i.e. the bending back motion velocity is slowing down. Note that the PME under visible irradiation is somewhat faster than the discoloration kinetic. From a quantitative point of view, the linear correlation between the two times is excellent (R^2=0.988) with the following equation:

$$VISIBLE \rightarrow \quad \tau_3^D = 70 - 1.8 * \tau_3^A \quad \#(3)$$

Regarding photocyclization, the process is more complex due to the involvement of two distinct time periods. The coloration kinetic involves a short time (τ_1^A< 3 min) and a longer time (τ_2^A<35 min) while the displacement is slower with also a short characteristic time (τ_1^D< 6 min) that contrasts with a longer time (τ_2^D< 50 min). If both times evolve along the cycle numbers, only the second time correlates properly (R^2=0.85) with a similar equation compared to the previous case.

$$UV \rightarrow \tau_2^D = 80 - 1.5 * \tau_2^A \quad \#(4)$$

The similarity between equation (3) and equation (4) testifies quantitatively for the reversibility of the photomechanical effect attributed to the reversibility of the photochromic reaction. In the near future, one has to rationalize the physic-chemical origin of both intercept and slope values of both correlation equations with the final idea to optimize the material performances (quantitative structure-property relationship).

2.3. Composition variation

i) Photochromic unit concentrations. In this study, thin films with varying molar ratios of photochromic units (A:B) were used to examine their effect on displacement tracking. Figure 3a shows the backward/forward displacement for thin films 1:1, 1:2, 1:3, and 1:5. Although the displacement is similar to the reference case (1:1), the amplitudes are different. Considering, for example, Cycle #3 (Figure 3b), the maximum displacement reached during UV or Vis irradiation of each film is plotted against the molar ratio. It is clear that, even though the curves are slightly different for either the UV or the visible illumination, the general result is simple: the PME is proportional to the content of A units. The photomechanical effect (PME) is directly proportional to the concentration of photoswitch units, whether under UV or visible illumination. Therefore, higher concentrations of photoswitch units result in a stronger PME.

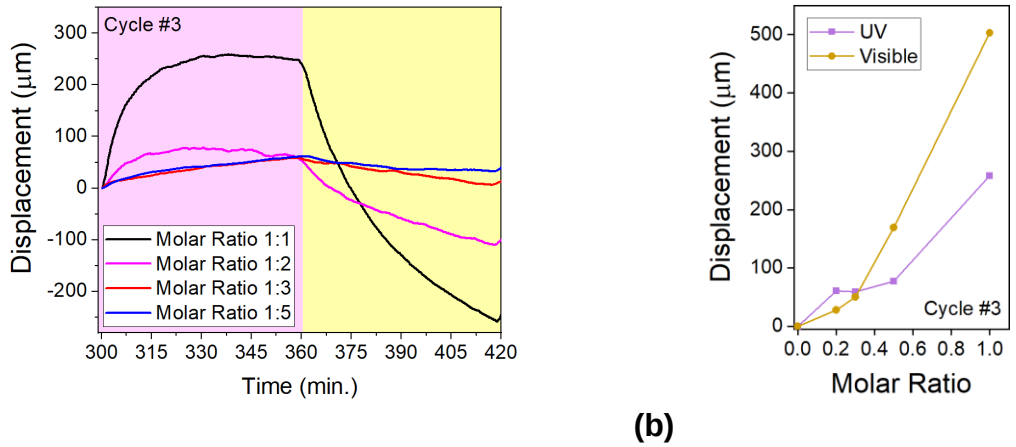

Figure 3. (a) Displacement tracking profiles (Cycle #3) for a series of thin films with different molar ratios (A: B) with approximately the same thickness. (b) Maximum displacement vs molar ratio.

ii) UPy Network. The role of the UPy-UPy hydrogen bonding network has been performed by the comparison of the displacement tracking profile of two thin films containing the same photochromic unit A but with different elastomers: i) the regular elastomer B, previously used, and ii) a novel elastomer where only 50% of chain-ends of the PEB were functionalized by a UPy unit, (B_{50}). The displacement tracking profiles of the two thin films (A/B) and (A/B_{50}) are displayed in Figure 4a using the same scale.

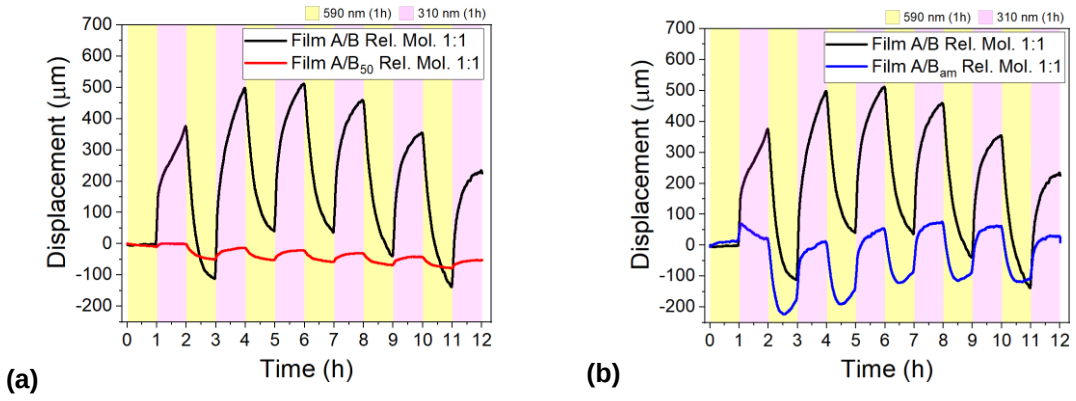

Figure 4. a) Displacement tracking profiles comparing thin film (A/B) (black line) and thin film (A/B_{50}) (red line). b) Displacement tracking profiles comparing semi-crystalline thin film (A/B) (black line) and amorphous thin film (A/B_{am}) (blue line).

Clearly, the first striking result concerns the drastic decrease in the PME amplitudes for both UV and visible excitations. When only 50% of chain-ends of PEB are functionalized with a UPy unit the PME amplitudes are reduced by an average factor of ~15 for UV and ~12 for visible excitation. Concerning the dynamic analysis comparing both systems (A/B) and (A/B_{50}) (see Table S1), it is striking to observe for photocyclization a quite similar behavior for cycle #2 followed by a drastic decrease of τ_2 (50 to 16 min) for the (A/B_{50}). Surprisingly, the characteristic times for visible excitation are of the same order of magnitude for both systems. In conclusion, to obtain a large PME and avoid a drastic attenuation effect, it is necessary to have UPy groups at both chain ends of the PEB, which form efficient UPy dimer domains.

iii) Microstructure. To investigate the effect of PEB elastomer crystallinity, we compared the displacement tracking profiles of a previous thin film (A/B) with a modified version using an amorphous elastomer (B_{am}) instead of the semicrystalline elastomer (B), as shown in Figure 4b. *The amorphous nature of B_{am} compared to its crystalline analog is demonstrated on WAXS results (see Supporting Information S6)* The well-know crystalline peaks related to polyethylene crystallite [REF] disappeared leaving only an amorphous halo which show unambiguously the amorphous microstructure of B_{am}. The amorphous thin film exhibits a similar back-and-forth displacement under successive UV/visible irradiation compared to the (A/B) system, but there are also some significant differences. First, PME amplitudes were divided by an average factor of 2.7 for UV and 2.5 for visible, respectively. Regarding the kinetic aspects (refer to Table S2), the photoreversion time τ_3 was again minimally affected by the microstructure change, while a drastic decrease for the

photocyclization was observed (time τ_2) with the amorphous microstructure (τ_1 was minimally affected). However, the most notable finding is the emergence of a new process. During visible illumination periods, the film bends towards the light direction, resulting in mechanical relaxation. This relaxation occurs after 20 minutes of irradiation and may be due to a rapid reorganization of the elastomeric network, causing rearrangement in packing and generating a smaller displacement. The displacement profiles were fitted with linear functions, and their slopes are given in Table S2. It is important to recall that partially crystalline elastomer B is crosslinked due to UPy-UPy aggregates interaction, while crystalline domains come mainly from polyethylene crystallinity. On the contrary, the B_{am} elastomer has the same crosslinking produced by the interaction between UPy-UPy aggregates, but since the polybutylene content is higher concerning the polyethylene, it does not have crystalline domains, being mostly amorphous. Therefore, the comparison of the two samples shows that the semicrystalline of the elastomer is not necessary to obtain PME, but it does increase the amplitude of the collective effect, probably due to relaxation minimization. Furthermore, the presence of semicrystalline domains prevents the attenuation of the collective effect during successive irradiations.

2.4 Structure and Morphology

In this section, we envision to rationalize from a structural and morphological point of view, the PME obtained for the thin film (A/B) with the aid of different techniques by comparing the OF and CF samples or implementing in-situ illumination during the measurement.

Microscopy. AFM analysis was performed on a single film (A/B) exposed to in situ illumination. Images were taken of the same area before illumination, after 1 hour of UV exposure, and finally after 1 hour of visible irradiation. The three AFM images (2 x 2)μm^2 are displayed in Figure 5a-c. Although no regular features are present and a slight shift occurs between images, it is possible to identify a common point on each image (marked with a white crosshair). Figure 5d uses this reference point to compare the height profiles extracted along the z-axis (height) and integrates the area under the curves (within the dashed rectangle). It is observed that after UV irradiation, the height profile of the film increases by 42%. This effect is attributed to the OF→CF photocyclization. After switching the sample back to the OF state using visible light, there was a significant decrease in peak height, resulting in a reduction of approximately 40% of the curve area. These results provide

evidence for reversible photoinduced expanding/contracting of the domains containing DTE, at least at the surface of the thin film.

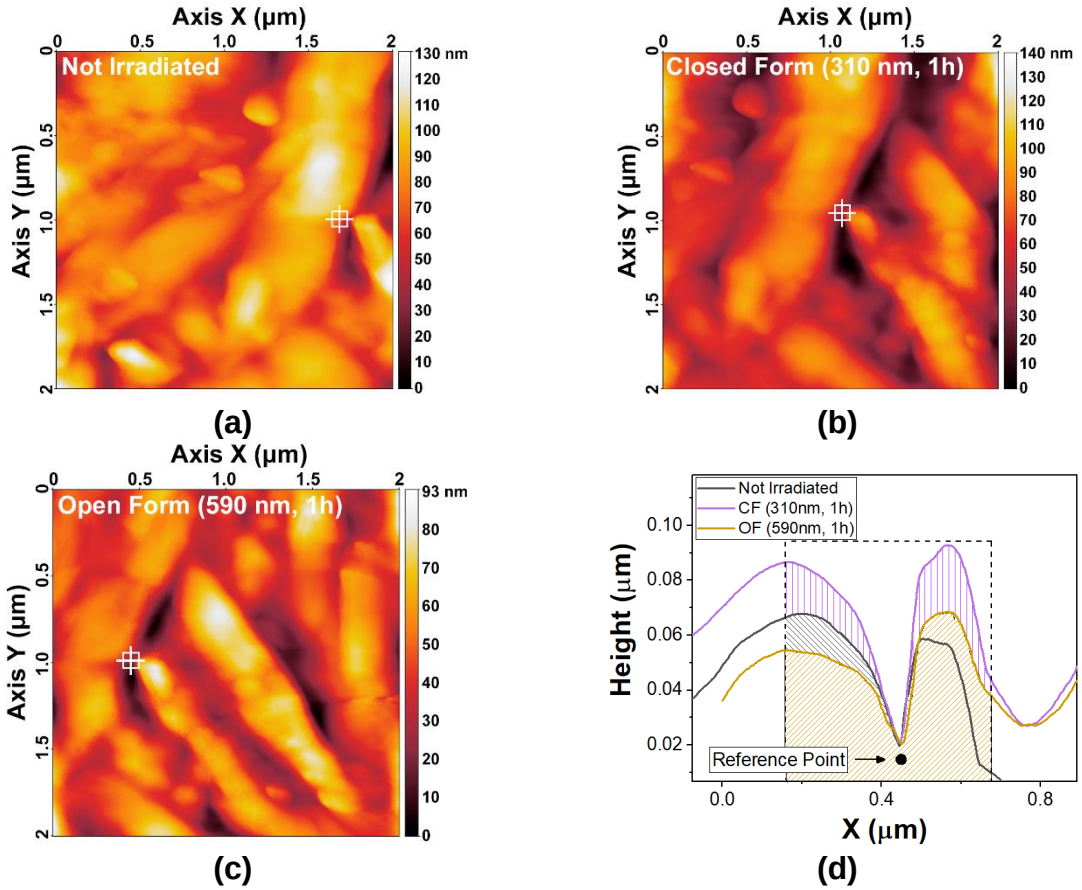

Figure 5. AFM images, (a) film (A/B) not irradiated, (b) film irradiated with UV light at 310 nm for one hour, and (c) same film irradiated with visible light at 590 nm for one hour. The power of both LED lamps was set to 1 mW.cm^{-2}. d) Comparison of the area obtained in each of the height profiles (on the X axis) for the AFM images (not irradiated, CF, and OF), using as reference the point shown as a white crosshair.

To corroborate these latter results, SEM analysis was performed on two samples from the same thin film (A/B) after 3 hours of UV (CF) or visible (OF) exposure. Because the surface of the samples is non-conductive, each sample was carbon coated (thickness of about 200 Å). Both OF and CF SEM images are displayed in Figure 6. The OF image displayed a non-uniform topography with domains of irregular morphology but with well-defined boundaries. In contrast, the CF sample exhibits a more rugged, irregular topography with irregularly shaped domains and poorly defined boundaries. At first sight, the domain size appears to be smaller in OF compared to CF. Indeed, the quantitative analysis illustrated in Figure 6c reveals that the average diameter distribution for OF is 163 nm with a standard deviation of 43 nm, whereas CF has an average diameter of 250 nm and a standard deviation of 96 nm. The SEM analysis indicates that CF domains are 53% larger than OF domains in perfect agreement with the AFM results.

Before going further, the question of the exact location of the photochromic units inside the elastomeric matrix has to be address. The elemental EDX maps of sulfur is displayed on figure S9 for OF and CF the latter element being indicative of the presence of A molecule slolely. At first glance, at the micrometric scale, the sulfur atoms are distributed homogeneously at the surface of both samples OF and CF. With this technics, we cannot distinguish the presence of domains outlined with SEM images and AFM analyses. (As expected, the atomic emission Kα spectra (not shown) also indicates that the concentrations of S are similar in both samples). However, by zooming the image, we are able to distinguish region without photochromic units with ranging less than 100 nm size. The contrast between the domain with and without photochromic units is probably an important factor to rationalize the PME.

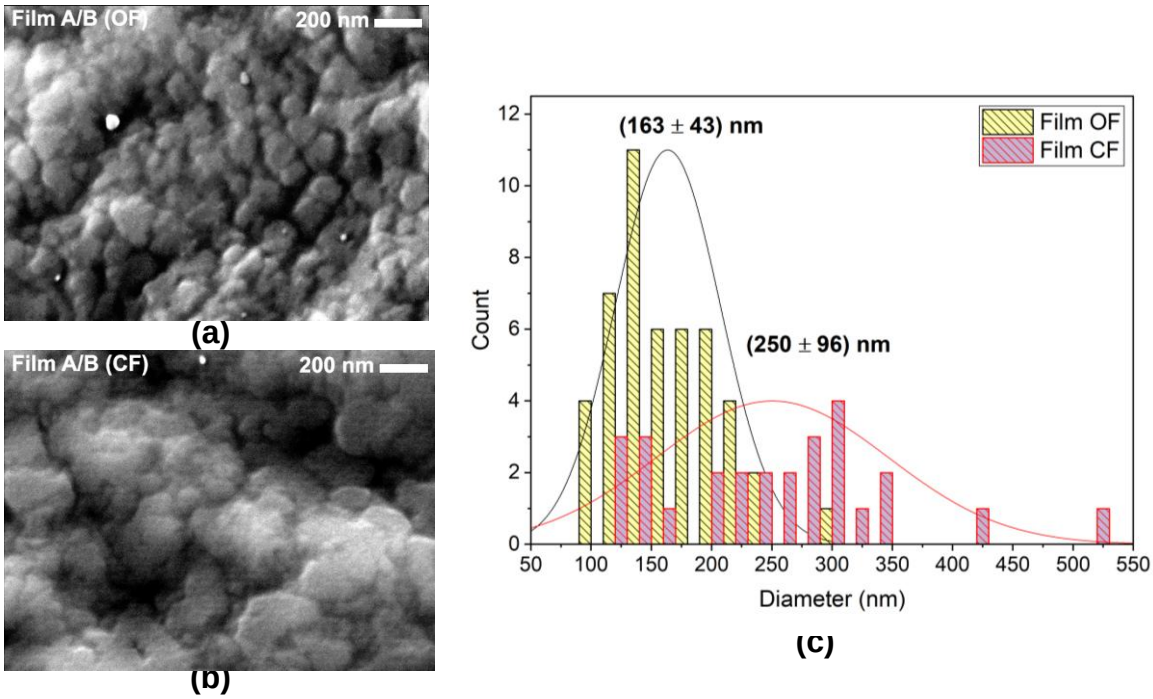

Figure 6. SEM images thin films (A/B) in a) Open Form and b) Closed Form. c) Domain size distribution

Scattering. Our group has previously conducted a comprehensive study on the same thermoplastic (poly(ethylene-co-butylene) elastomer thin film B but for different processing protocols (drop casting, thermal molding).[65] With the WAXS technique, we have reported first the full description of the crystalline structure of polyethylene segments in either orthorhombic or monoclinic forms.[73–75] As expected, functionalizing the thermoplastic elastomer with UPy unit results in a supramolecular network that creates a competition between the natural organization of the elastomer (dependent on the copolymer ethylene/butylene ratio) and the organization of the macromolecules via quadruple hydrogen bonding. Indeed, the microstructure of the supramolecular network has been revealed by a weak feature assigned to the interplanar distance of 1 nm between UPy near neighbors[76]

(dimers)With the SAXS technique, a clear microphase separation has been reported between polyethylene segments and UPy-UPy domains (see the two peaks in SAXS, Fig. 4, Louati *et al.*[65]). We are now interested to rationalize the interaction between A and B by analyzing SAXS and WAXS spectra with in-situ illumination.

To gain a thorough comprehension of our system, we conducted WAXS and SAXS analyses using an *in situ* illumination sequence, depicted in Figure 7. This was done by taking a spectrum before illumination, a spectrum after 1 hour of UV irradiation, and ending with taking a spectrum after 1 hour of visible irradiation. The deconvoluted WAXS spectra (refer to Supporting Information SI6) revealed the presence of five peaks, in addition to a large corresponding to an amorphous fraction. Four of the five peaks correspond to the crystalline fractions of polyethylene: two peaks at 2θ=21.3° and 23. 5° correspond to the (110) and (200) planes of the orthorhombic form (a=7.40 Å, b=4.93 Å, and c=2.54 Å), while the peaks at 2θ=19.5° and 23.1° are associated with the (001) and (002) planes of the monoclinic form (a=8.09 Å, b=4.79 Å, c=2.53 Å, and β=107°).[65,77–79] Following our preliminary results, the small peak at 2θ=8.1° corresponding to the reflection of the stacked planes of the UPy domains at d=1 nm is detected.[55,76,80] The crystallinity and the relative fractions of the crystalline phases were calculated from the integrated areas of the corresponding peaks. The orthorhombic fraction represents 75% while the monoclinic fraction represents 25% of the overall crystallinity. A comparison of the three spectra under the influence of light revealed no differences in peak shape or intensities, and the overlap of the three spectra was perfect. Therefore, the packing of the ordered parts of the supramolecular network remained unaltered during the illumination sequence.

In contrast, the structureless SAXS spectra presented in Figure 7b are responsive to irradiation which demands a careful analysis. As already reminded above, the elastomer B (drop cast thin film) alone[65] presents two distinct peaks attributed to a microphase separation between the polyethylene crystallites and UPy domains. Introducing the photochromic unit A significantly disrupts this microphase separation as evidenced by the disappearance of one of the peaks for the SAXS spectra of the A/B system. Then, as seen in Figure 7b, the effect of successive UV/visible illumination sequences (1h duration) on the photoactuator A/B is quite striking. The results can be summarized as follows: i) the high-q contribution spectra increase in intensity after receiving 1h UV irradiation, while the low-q contribution remains constant; ii) the process is reversible as, after a subsequent 1h long illumination under visible light, the scattering curve returns to the initial state. In fact, the

SAXS profile before irradiation can be interpreted as the sum of two contributions. On the one hand, at low q (i.e. below 5.10^{-2} $\dot{A}^{-1}$) the scattered intensity steadily increases with the decrease of q. This contribution is attributed to the scattering from a large size structure which cannot be determined here due to the limited low q-range accessible. On the other hand, the scattering signal at $q > 5.10^{-2}$ $\dot{A}^{-1}$ can be attributed to the scattering arising from the UPy stacks.

Upon UV illumination only changes regarding the scattered intensity at "high" q are observed. More precisely, while the shape of the curve remains the same, only the intensity of the curve increases. Considering that this part of the curve originates from the scattering of the UPy stacks, this intensity change can be interpreted by a change in electronic contrast between the UPy stacks and the surrounding matrix. Indeed, the scattered intensity I(q) can be expressed as:

$$I(q) \propto \Delta\rho^2 . S(q) . F(q) \#(5)$$

With $\Delta\rho^2$, the difference of electronic density between the scatterer (i.e., the UPy stacks) and the matrix; F(q) being the form factor which corresponds here to the shape of the UPy stacks; S(q) being the structure factor which corresponds to a potential regular arrangement between the scatterers (assumed here to be neglected due to the low concentration of UPy).

The reversible increase or decrease of the SAXS signal observed upon UV/visible irradiation reflects a change in the electronic density of the UPy stacks containing the photoswitch units. The OF molecule is known to be more flexible (with free libration of thiophene moieties) than the rigid CF molecule, implying a better conformational adaptation to the environment, in contrast to CF analogs that push apart the hydrogen-bonded UPy dimers. Furthermore, the electronic density of the photochromic core of CF is stronger than that of the electron densities isolated on the two thiophene moieties of OF.[30] Therefore, the reversible change in electronic density detected by SAXS can be attributed to the conformational/electronic density change from OF to CF of photochromic units engaged in UPy domains.

In conclusion, by gathering together the AFM, SEM, and SAXS results, the PME is explained in terms of photoinduced reversible contraction/expansion of UPy domains diameter of ~160 nm containing the photochromic units which expand under UV (rigid with high electronic density CF) up to ~250 nm and reversibly contract under visible light (flexible low electronic density OF). Those domains are illustrated by the colored circles in Figure 7c.

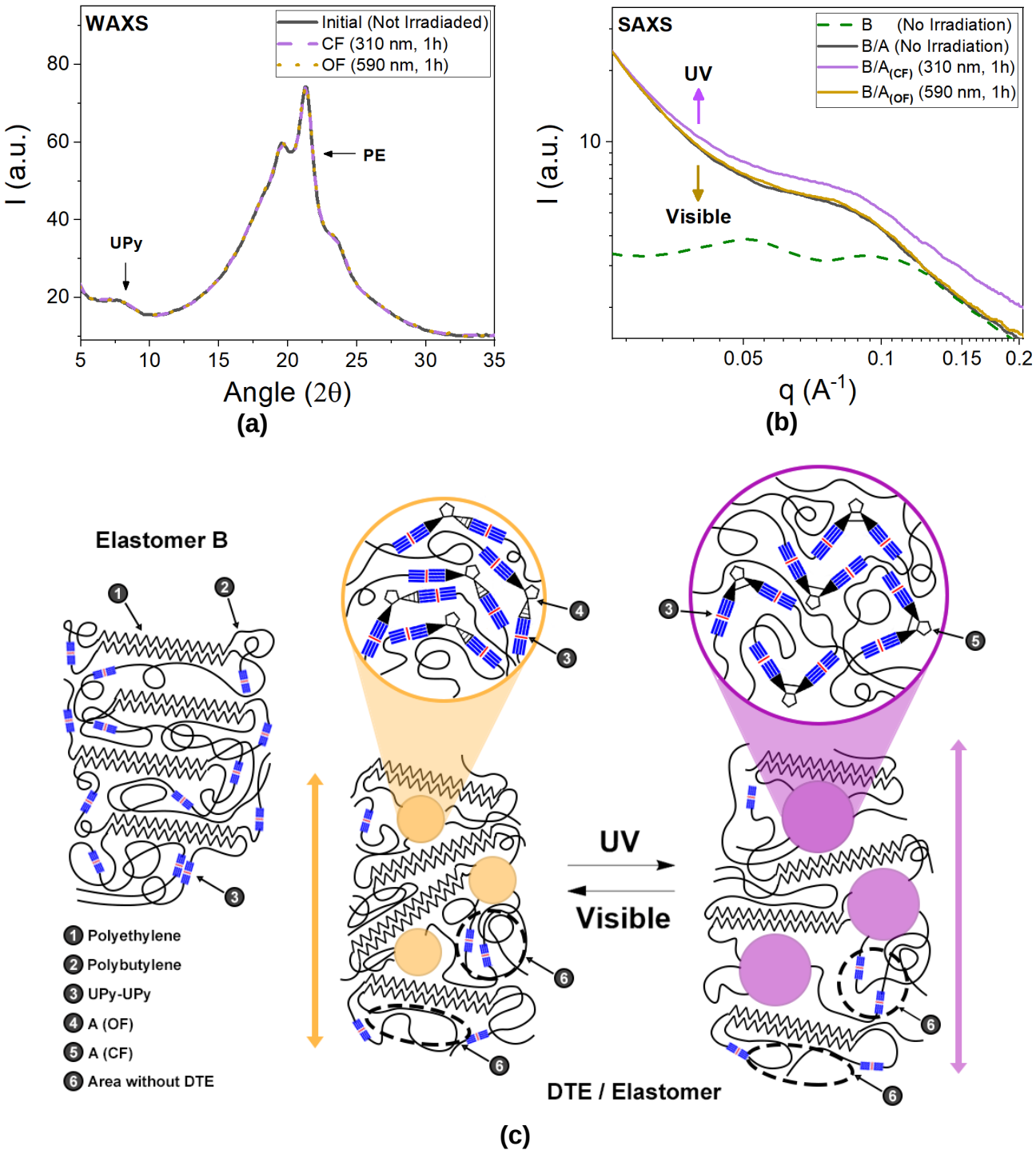

Figure 7. a) WAXS intensity profiles and b) SAXS scattering profiles for thin films (A/B) before irradiation, after 1 hour of UV irradiation (CF), and after 1 hour of visible irradiation (OF). For comparison, SAXS scattering profiles for a thin film of pure B (Intensity divided by 2). c) Schematic organization of thin film B (microphase separation) and thin film (A/B) with the photochromic unit in OF or CF.

2.5 Rationalization of the PME.

Throughout this manuscript, it has been shown that photomechanical behavior can be obtained in a centimeter (A/B) photoactuator with a supramolecular approach based on UPy units. Strong evidence suggests that photoswitching DTE units lead the entire system during the photoactuation process, as long as the duration of the illumination sequence is faster than the matrix relaxation. The efficiency of photochromic units to propagate their actuation around their environment is so strong that it is reasonable to make an analogy between pure DTE crystal photoactuators[15,81] and thin film (A/B). This analogy is illustrated in Figure 8. Both crystalline and elastomeric photoactuators rely on the same property of DTE, namely, the variation in flexibility in contrast to its rigidity and the change in molecular size in its different states. Irie et al. demonstrated this phenomenon over a decade ago by characterizing the structure of DTE crystals. Their crystallographic measurements of OF and CF revealed elongation of a specific crystallographic axis under UV irradiation, while other planes remained unaffected by light.[70] In addition to the above results, our novel A/B system, despite the lack of long-range order between the DTE units, the expansion and contraction of the UPy domains of the photochromic units surrounded by amorphous matter shows that it is not a well-defined crystalline order that is necessary to obtain PME.[72] However, it is important to consider that the semicrystalline fraction within the polymer matrix plays a crucial role in the propagation of photostrain throughout the material. As a result, it is highly correlated with the efficiency of the photoactuator.

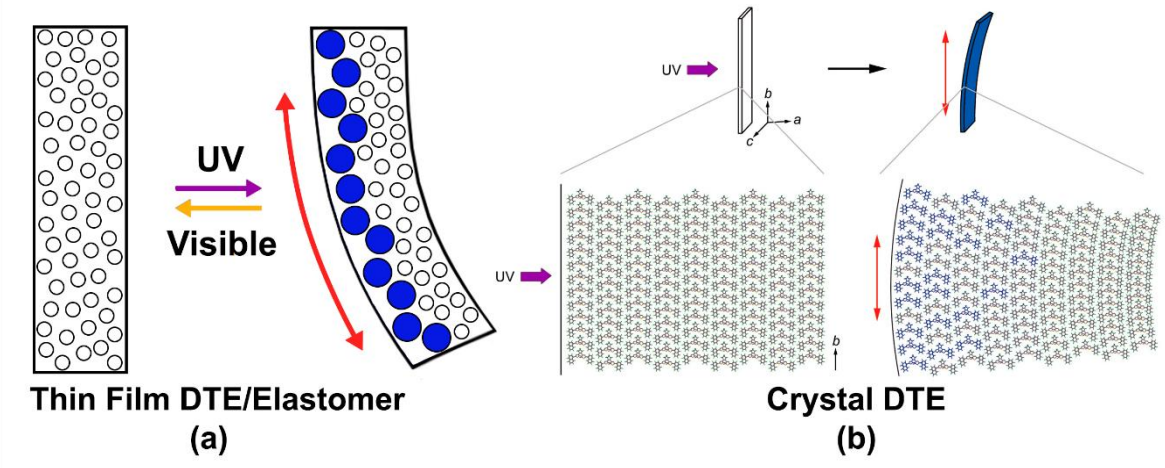

Figure 8. a) Bending of a thin film (A/B) in the direction of light by increasing the size of the domains from OF to CF b) Schematic illustration of the photoinduced bending. The blue molecules are photogenerated closed-ring isomers in the crystal. Reprinted (adapted) with permission from M. Morimoto and M. Irie, "A Diarylethene Cocrystal that Converts Light into Mechanical Work," J. Am. Chem. Soc., vol. 132, no. 40, pp. 14172–14178, Oct. 2010, doi: 10.1021/ja105356w. Copyright 2023 American Chemical Society.

3. Conclusion

PME of polymeric systems is promising to achieve controlling matter using light. As an alternative to either AZO-LCE or crystalline DTE photoactuators, a novel supramolecular approach has been investigated by combining a semi-crystalline thermoplastic elastomer B and a photochromic unit A, both of which are functionalized with UPy units to allow a strong quadruple hydrogen bonding between the two components A and B. In contrast to the complicated and energy-intensive protocols required for either the LCE system (photopolymerization, thermal stretching, etc.) or the crystalline DTE (several days of recrystallization), the thin film (A/B) is easily and rapidly prepared by simple spin-coating from solution.

The breakthrough idea of this study is to restrict the PME to the unique actuation originating from the photochemistry of DTE alone far from the thermal requirements of LCE systems. In this sense, we have shown that a strong analogy can be built between crystalline DTE and our system that includes an additional elastomer and paves the way to build centimetric systems.

From a structural point of view, it has been found with several material science techniques that the thin film (A/B) is crosslinked with both polyethylene crystallite and UPy domains (~160 nm). The PME relies on the well-known property of flexibility of the OF contrasting with the rigidity of the CF after electrocyclization of the photochromic core. As a consequence, the UPy domains containing DTE molecules expand by about 50% under UV and reversibly retract under visible irradiation. The most important parameters to get an efficient PME are i) a good hydrogen-bonded UPy network to avoid the microphase separation between PEB chains and DTE units; ii) the presence of semi-crystalline polyethylene segments that help to amplify the PME initiated inside the UPy domains containing the photoswitch and restricting damping effect.

Finally, we can expect to improve the performances in the future by following several routes: i) molecular design of both elastomer and DTE with the idea to control the local structure of the UPy domains; ii) choosing dissymmetric illumination period to take into account the specific photochemistry of OF and CF species. iii) increasing the LED power to combine both photochemical and photothermal effects. Such material optimizations as well as advanced mechanical measurements are now under investigation in our laboratories.

4. Experimental Section

Films preparation

The films were prepared from a polymer solution based on a mixture of A and B (or B_{50}, Bam) in chloroform. A molar ratio (A:B) of 1:1 was used with a relative amount between A and chloroform of 33 wt%. The solution was stirred at reflux for 1 hour and then sonicated for 15 minutes. The solution was then dropped (at room temperature) onto a silica paper substrate and spin-coated (APT, mod: SPIN150) at 200 rpm for 150 seconds (the thickness of the films obtained was about 20 µm). The polymer films obtained were cut into small rectangles of (10 x 2) mm^2 for subsequent analysis and characterization.

General characterizations

Illumination system. The illumination system consisted of two LED lamps with collimated light. They were placed 7 cm away from the film with a 60° angle between the two lamps. A LED lamp (MIGHTEX LCS 0590-03-22) with a wavelength of 590 nm was used for visible light, while for UV light a LED lamp (MIGHTEX LCS 0310-03-23) with a wavelength of 310 nm was used. An LED driver (MIGHTEX SLA-1000-2) was used to control the intensity of both lamps. For all analyses, the intensity of the visible light and the UV light was adjusted to 1 mW.cm-2.

Displacement tracking video setup. Before each analysis, the film (10 x 2 x 0.017) mm^3 was suspended in the fixation system and fixed with clamps for 24 hours without any manipulation to avoid mechanical relaxation effects. The bending of the films during the illumination cycles of the LED lamps was recorded in time-lapse video, each frame (photo) each second. The video was recorded using an electronic industrial microscope consisting of a HAEYER mod: HY-1138 with a 30 MP camera and a 300X objective. Both the camera and the LED lamps were controlled by LABVIEW, a National Instrument USB-6501 controller, and a dedicated program. All measurements were performed in the air and carried out at room temperature. All samples were subjected to multiple actuation conditions to verify the reversibility and reproducibility of the bending changes. The tracking profile analysis was performed using Adobe After Effects software on the recorded videos. Details of the displacement calculation can be found in supporting information S3.

***Absorbance and absorbance tracking profile*.** The steady-state absorption spectra of the films were obtained using a double-beam VARIAN spectrometer (CARY100 bio-visible) with a spectral range of 200 to 800 nm. For thin film spectra, the air was used as a reference. The real-time absorbance tracking profile for the films (A/B) was performed in situ with an OPHIR power meter (StarBright, 7Z01580) using a photodiode (PD300R-UV) with a spectral range from 200 to 1100 nm and a power measurement range from 20 pW to 3 mW. A THORLABS laser (PL202) with a wavelength of 635 nm was used as the excitation medium, to which a filter lens with an optical density of 2 (OD=2) was added to reduce the laser intensity and avoid photoreversion. A 635 nm laser line filter (THORLABS, FL635-10) was placed in front of the photodiode to avoid contributions to the absorbance measurement from the visible LED.

Material science technics. Wide-angle X-ray scattering (WAXS) and small-angle X-ray scattering (SAXS) experiments were performed on a Xeuss 2.0 (Xenocs) operating under vacuum with a GeniX3D microsource (λ = 1.54 Å) at 0.6 mA and 50 kV and a 2D Pilatus 3 R 200 K detector. The analyses were performed in transmission mode. The WAXS patterns were acquired with a sample-to-detector distance of 160 mm, while the SAXS detector was positioned at 2300 mm from the sample. From the patterns, the WAXS and SAXS scattered intensities were integrated and plotted against the scattering angle 2θ and the scattering vector $q = (4\pi/\lambda)\sin\theta$, respectively. In-situ illumination was implemented using the illumination system described above.

Morphological analysis was performed using a JEOL JSM 7800F LV (Electron Microscopy Platform). The secondary electron images to document the surface morphology were acquired with 2kV acceleration voltage, low probe current value (below 100 pA), and 10mm working distance to avoid polymer degradation. Prior to observation, the films were fixed on an aluminum stub with conductive carbon adhesive tape, and carbon deposit (~200 Å) was carried out using a carbon evaporator to make the surface conductive. Because of the carbon deposition, in-situ illumination was not possible, and SEM images of the OF and CF samples were taken separately (with illumination before the carbon deposit). Chemical elemental Energy-dispersive X-ray (EDX) analyses were conducted with an accelerating voltage of 5keV using a X-Max SDD (Oxford Instruments) detector. The EDX maps were treated and extracted using the software Aztec 6.1 (Oxford Instruments). AFM analysis was performed with an NTEGRA mod. NT-MDT in semi-contact mode with a silicon cantilever with gold coating NTEGRA, mod. NSG30 and an oscillation frequency of 278.34 Hz. The

images were taken on the films without any surface preparation, at atmospheric pressure and room temperature. In-situ illumination was implemented using the illumination system described above. The scanned areas were 2 μm x 2 μm with a resolution of 1024 x 1024 lines. Analysis was performed using Gwyddion software (open source).

Acknowledgments

The authors are grateful to "Agence National pour la Recherche" through the project ANR-19-CE06-0022 – TACTIL for the funding of this research (PhD salary and equipment). The authors are also grateful to Région Haut-de France for partially granting a PhD fellowship to M. Arroyo-Diaz. Chevreul Institute (FR 2638), Ministère de l'Enseignement Supérieur, de la Recherche et de l'Innovation, Région Hauts de France and FEDER are acknowledged for supporting and funding the SAXS/WAXS analysis. Special thanks to Dr. Gregory Stoclet for his decisive help in interpreting the SAXS spectra.

Conflict of Interest

The authors declare no conflict of interest.

Author Contributions

IA has undertaken the overall experiments of this manuscript. He has built up the video tracking profile setup and homemade analysis. He has written a large part of this article and elaborated on figures, tables, and video. RC has built up the beta version of the absorbance tracking profile. Synthesis of molecule A (GA), molecule B (DF), molecule Bam (NNE and SP), and molecule B_{50} (MT). AF has performed MEB measurements. JFT and SB have launched SAXS/WAXS measurements. GB and MN-A have given their expertise in optics and mechanics respectively. LB reviewed the article several times highlighting a straightforward idea based on his material science expertise. SA was the supervisor of IA; he has written a large part of this article and has managed the different contributions. All authors have approved the final version of the manuscript.

Data Availability Statement

The data that support the findings of this study are available from the corresponding author upon reasonable request.

References

[1] W.A. Phillip, Nature Energy 1 (2016) 16101.
[2] C. Cheng, A.H.W. Ngan, ACS Nano 9 (2015) 3984–3995.
[3] M.R. Islam, X. Li, K. Smyth, M.J. Serpe, Angewandte Chemie International Edition 52 (2013) 10330–10333.
[4] Y. Hu, Z. Li, T. Lan, W. Chen, Advanced Materials 28 (2016) 10548–10556.
[5] M. Shahinpoor, Fundamentals of Smart Materials, Royal Society of Chemistry, 2020.
[6] P. Wang, Smart Materials for Advanced Environmental Applications, Royal Society of Chemistry, 2016.
[7] C.K. Soh, Y. Yang, S. Bhalla, Smart Materials in Structural Health Monitoring, Control and Biomechanics, Springer Berlin Heidelberg, 2012.
[8] A. Filimon, Smart Materials: Integrated Design, Engineering Approaches, and Potential Applications, Apple Academic Press, 2018.
[9] H. Koshima, Mechanically Responsive Materials for Soft Robotics, Wiley, 2020.
[10] S. Schneegass, O. Amft, Smart Textiles: Fundamentals, Design, and Interaction, Springer International Publishing, 2017.
[11] Q. Li, Photoactive Functional Soft Materials: Preparation, Properties, and Applications, Wiley, 2018.
[12] H. Miyasaka, K. Matsuda, J. Abe, T. Kawai, Photosynergetic Responses in Molecules and Molecular Aggregates, Springer Singapore, 2020.
[13] T.J. White, Photomechanical Materials, Composites, and Systems: Wireless Transduction of Light into Work, 2017.
[14] Y. Yu, M. Nakano, T. Ikeda, Nature 425 (2003) 145–145.
[15] F. Tong, D.-H. Qu, Langmuir 38 (2022) 4793–4801.
[16] T.J. White, Journal of Polymer Science Part B: Polymer Physics 50 (2012) 877–880.
[17] P.-F. Luo, S.-L. Xiang, C. Li, M.-Q. Zhu, Journal of Polymer Science 59 (2021) 2246–2264.
[18] T. Naito, K. Horie, I. Mita, Macromolecules 24 (1991) 2907–2911.
[19] P. Uznanski, M. Kryszewski, E.W. Thulstrup, European Polymer Journal 27 (1991) 41–43.
[20] L. Dong, Y. Zhao, Mater. Chem. Front. 2 (2018) 1932–1943.
[21] Z. Ren, K. Ding, X. Zhou, T. Ji, H. Sun, X. Chi, M. Xu, International Journal of Biological Macromolecules 253 (2023) 126562.
[22] M. Irie, Proc Jpn Acad Ser B Phys Biol Sci 86 (2010) 472–483.
[23] P. Naumov, D.P. Karothu, E. Ahmed, L. Catalano, P. Commins, J. Mahmoud Halabi, M.B. Al-Handawi, L. Li, J. Am. Chem. Soc. 142 (2020) 13256–13272.
[24] P. Naumov, S. Chizhik, M.K. Panda, N.K. Nath, E. Boldyreva, Chem. Rev. 115 (2015) 12440–12490.
[25] T. Kim, L. Zhu, R.O. Al-Kaysi, C.J. Bardeen, ChemPhysChem 15 (2014) 400–414.
[26] Y. Hu, Z. Li, T. Lan, W. Chen, Advanced Materials 28 (2016) 10548–10556.
[27] J. Li, X. Zhou, Z. Liu, Adv. Optical Mater. 8 (2020) 2000886.
[28] W. Francis, A. Dunne, C. Delaney, L. Florea, D. Diamond, Sensors and Actuators B: Chemical 250 (2017) 608–616.
[29] J.E. Angulo-Cervera, M. Piedrahita-Bello, B. Brachňaková, A. Enríquez-Cabrera, L. Nicu, T. Leichle, F. Mathieu, L. Routaboul, L. Salmon, G. Molnár, A. Bousseksou, Mater. Adv. 2 (2021) 5057–5061.
[30] M. Irie, T. Fukaminato, K. Matsuda, S. Kobatake, Chem. Rev. 114 (2014) 12174–12277.
[31] Y. Zhao, T. Ikeda, Smart Light-Responsive Materials: Azobenzene-Containing Polymers and Liquid Crystals, Wiley, 2009.
[32] G.S. Kumar, D.C. Neckers, Chem. Rev. 89 (1989) 1915–1925.
[33] E. Merian, Textile Research Journal 36 (1966) 612–618.
[34] F. Agolini, F.P. Gay, Macromolecules 3 (1970) 349–351.
[35] H.M.D. Bandara, S.C. Burdette, Chem. Soc. Rev. 41 (2012) 1809–1825.
[36] M. Warner, E.M. Terentjev, Liquid Crystal Elastomers, OUP Oxford, 2007.
[37] M.W. Urban, Handbook of Stimuli-Responsive Materials, Wiley, 2011.
[38] T.S. Hebner, C.N. Bowman, T.J. White, Polym. Chem. 12 (2021) 1581–1587.

[39] T. Ikeda, M. Nakano, Y. Yu, O. Tsutsumi, A. Kanazawa, Advanced Materials 15 (2003) 201–205.
[40] L.A.E. Müller, A. Demongeot, J. Vaucher, Y. Leterrier, J. Avaro, M. Liebi, A. Neels, I. Burgert, T. Zimmermann, G. Nyström, G. Siqueira, ACS Appl. Mater. Interfaces 14 (2022) 16703–16717.
[41] H. Finkelmann, E. Nishikawa, G.G. Pereira, M. Warner, Phys. Rev. Lett. 87 (2001) 015501.
[42] T. Ikeda, J. Mamiya, Y. Yu, Angewandte Chemie International Edition 46 (2007) 506–528.
[43] T. Ikeda, J. Mater. Chem. 13 (2003) 2037–2057.
[44] M. Yamada, M. Kondo, J. Mamiya, Y. Yu, M. Kinoshita, C.J. Barrett, T. Ikeda, Angewandte Chemie International Edition 47 (2008) 4986–4988.
[45] T. Ube, H. Tsunoda, K. Kawasaki, T. Ikeda, Advanced Optical Materials 9 (2021) 2100053.
[46] J.J. Wie, M.R. Shankar, T.J. White, Nature Communications 7 (2016) 13260.
[47] M. Lahikainen, K. Kuntze, H. Zeng, S. Helantera, S. Hecht, A. Priimagi, ACS Appl. Mater. Interfaces 12 (2020) 47939–47947.
[48] T.S. Hebner, M. Podgórski, S. Mavila, T.J. White, C.N. Bowman, Angewandte Chemie International Edition 61 (2022) e202116522.
[49] J. Zhao, L. Zhang, J. Hu, Advanced Intelligent Systems 4 (2022) 2100065.
[50] T. Ube, R. Nakayama, T. Ikeda, Macromolecules 55 (2022) 413–420.
[51] Y. Wu, Y. Yang, X. Qian, Q. Chen, Y. Wei, Y. Ji, Angewandte Chemie International Edition 59 (2020) 4778–4784.
[52] T. Ube, K. Kawasaki, T. Ikeda, Advanced Materials 28 (2016) 8212–8217.
[53] Y. Zhu, M. Zheng, Y. Tu, X.-F. Chen, Macromolecules 51 (2018) 3487–3496.
[54] R.P. Sijbesma, E.W. Meijer, Chem. Commun. (2003) 5–16.
[55] D.K. Hohl, S. Balog, C. Cappelletti, F. Karasu, C. Weder, Macromolecules 53 (2020) 9086–9096.
[56] G. Berger, J. Soubhye, F. Meyer, Polym. Chem. 6 (2015) 3559–3580.
[57] Z. Zhou, X. Yan, T.R. Cook, M.L. Saha, P.J. Stang, J. Am. Chem. Soc. 138 (2016) 806–809.
[58] J.E. Koskela, V. Liljeström, J. Lim, E.E. Simanek, R.H.A. Ras, A. Priimagi, M.A. Kostiainen, J. Am. Chem. Soc. 136 (2014) 6850–6853.
[59] S. Cao, L. Song, H. Zhang, J. Han, Y. Zhao, Chinese Chemical Letters 34 (2023) 108479.
[60] Y. Takashima, Y. Sawa, K. Iwaso, M. Nakahata, H. Yamaguchi, A. Harada, Macromolecules 50 (2017) 3254–3261.
[61] R.P. Sijbesma, F.H. Beijer, L. Brunsveld, B.J.B. Folmer, J.H.K.K. Hirschberg, R.F.M. Lange, J.K.L. Lowe, E.W. Meijer, Science 278 (1997) 1601–1604.
[62] S.H.M. Söntjens, R.P. Sijbesma, M.H.P. van Genderen, E.W. Meijer, J. Am. Chem. Soc. 122 (2000) 7487–7493.
[63] B.J.B. Folmer, R.P. Sijbesma, R.M. Versteegen, J.A.J. van der Rijt, E.W. Meijer, Adv. Mater. 12 (2000) 874–878.
[64] H.M. Keizer, R. van Kessel, R.P. Sijbesma, E.W. Meijer, Polymer 44 (2003) 5505–5511.
[65] M. Louati, J.-F. Tahon, D. Fournier, G. Stoclet, S. Aloise, M. Takao, M. Takeshita, J.-M. Lefebvre, S. Barrau, Polymer 228 (2021) 123875.
[66] M. Takeshita, M. Hayashi, S. Kadota, K.H. Mohammed, T. Yamato, Chem. Commun. (2005) 761.
[67] M. Takeshita, M. Hayashi, T. Miyazaki, Chem. Lett. 39 (2010) 82–83.
[68] I. Hamdi, G. Buntinx, O. Poizat, A. Perrier, L. Le Bras, S. Delbaere, S. Barrau, M. Louati, M. Takeshita, K. Tokushige, M. Takao, S. Aloïse, J. Phys. Chem. A 122 (2018) 3572–3582.
[69] M. Irie, Photochem Photobiol Sci 9 (2010) 1535–1542.
[70] M. Morimoto, M. Irie, J. Am. Chem. Soc. 132 (2010) 14172–14178.
[71] V.M. Breslin, M.A. Garcia-Garibay, Crystal Growth & Design 17 (2017) 637–642.
[72] M. Louati, S. Barrau, J.-F. Tahon, A. Brosseau, M. Takao, M. Takeshita, R. Métivier, G. Buntinx, S. Aloise, Journal of Molecular Structure 1261 (2022) 132857.
[73] J.C. Wittmann, B. Lotz, Polymer 30 (1989) 27–34.
[74] L. Fontana, D.Q. Vinh, M. Santoro, S. Scandolo, F.A. Gorelli, R. Bini, M. Hanfland, Phys. Rev. B 75 (2007) 174112.
[75] V.F. Holland, Journal of Applied Physics 35 (1964) 3235–3241.
[76] W.P.J. Appel, G. Portale, E. Wisse, P.Y.W. Dankers, E.W. Meijer, Macromolecules 44 (2011) 6776–6784.

[77] T. Seto, T. Hara, K. Tanaka, Japanese Journal of Applied Physics 7 (1968) 31.
[78] Y. Takahashi, T. Ishida, M. Furusaka, J. Polym. Sci. B Polym. Phys. 26 (1988) 2267–2277.
[79] K.E. Russell, B.K. Hunter, R.D. Heyding, Polymer 38 (1997) 1409–1414.
[80] J.-L. Wietor, D.J.M. van Beek, G.W. Peters, E. Mendes, R.P. Sijbesma, Macromolecules 44 (2011) 1211–1219.
[81] Y.-L. Chen, Y.-G. Wang, Q. Yu, Organometallics 42 (2023) 2159–2170.